Zeolite GdNaY Nanoparticles with Very High Relaxivity for Application as Contrast Agents in Magnetic Resonance Imaging

Carlos Platas-Iglesias,[a, b] Luce Vander Elst,[c] Wuzong Zhou,[d] Robert N. Muller,[c] Carlos F. G. C. Geraldes,[e] Thomas Maschmeyer,[a] and Joop A. Peters*[a]

Abstract: In this paper we explore Gd^{3+}-doped zeolite NaY nanoparticles for their potential application as a contrast agent in magnetic resonance imaging (MRI). The nanoparticles have an average size of 80–100 nm, as determined by TEM and XRD. A powdered sample loaded with La^{3+} was characterised by means of multinuclear solid-state NMR spectroscopy. The NMR dispersion (NMRD) profiles obtained from aqueous suspensions of samples with Gd^{3+} doping ratios of 1.3–5.4 wt% were obtained at different temperatures. The relaxivity increases drastically as the Gd^{3+} loading decreases, with values ranging between 11.4 and 37.7 $s^{-1}mM^{-1}$ at 60 MHz and 37 °C. EPR spectra of aqueous suspensions of the samples suggest that an interaction between neighbouring Gd^{3+} ions within the same particle produces a significant increase in the transversal electronic relaxation rates in samples with a high Gd^{3+} content. The experimental NMRD and EPR data are explained with the use of a model that considers the system as a concentrated aqueous solution of Gd^{3+} in the interior of the zeolite that is in exchange with the bulk water outside the zeolite. The results obtained indicate that the Gd^{3+} ion is immobilised in the interior of the zeolite and that the relaxivity is mainly limited by the relatively slow diffusion of water protons from the pores of the zeolite channels into the bulk water.

Keywords: contrast agents · gadolinium · lanthanides · magnetic resonance imaging · zeolites

Introduction

The fast development of magnetic resonance imaging (MRI) as a diagnosis procedure has provoked an enormous interest in lanthanide complexes for application as contrast agents.[1–4] To be effective, MRI contrast agents must have a strong local effect on the proton relaxation rates ($1/T_1$ and $1/T_2$) of water (which determine the intensities of the MRI signal), have adequate pharmacokinetic properties and, obviously, be non-toxic. The ability to enhance proton relaxation rates in the tissue in which they are distributed is usually evaluated "in vitro" by the determination of their relaxivity, which refers to the relaxation enhancement of water protons promoted by a given complex at a concentration of 1 mM of the paramagnetic metal ion. Around a paramagnetic ion, the relaxation rates of the bulk water protons are enhanced as a result of long-range interactions (outer-sphere relaxation) and short-range interactions (inner-sphere relaxation). According to the standard Solomon–Bloembergen–Morgan model, the latter process is governed by four correlation times: the rotational correlation time of the complex (τ_R), the residence time of a water proton in the inner coordination sphere (τ_m), and the electronic longitudinal and transverse relaxation rates ($1/T_{1e}$ and $1/T_{2e}$) of the metal centre. The theory predicts that high relaxivities at the imaging fields (0.5–1.5 T) may be observed for systems with a long rotational correlation time and relatively fast water exchange.[1–4] Several approaches have been used to increase the τ_R values of paramagnetic complexes, including covalent binding to slowly tumbling substrates, such as dextran[5] or inulin,[6] formation of self-aggregates in solution[7, 8] and formation of noncovalent adducts with β-cyclodextrin[9] or albumin.[10]

Among current commercially available MRI contrast agents for clinical use are polyamino polycarboxylate complexes of Gd^{3+}, such as $[Gd(dtpa)(H_2O)]^{2-}$ (dtpa = diethyle-

[a] Dr. J. A. Peters, Dr. C. Platas-Iglesias, Prof. Dr. T. Maschmeyer
Laboratory of Applied Organic Chemistry and Catalysis
Delft University of Technology, Julianalaan 136
2628 BL Delft (The Netherlands)
Fax: (+31) 15 2784289
E-mail: j.a.peters@tnw.tudelft.nl

[b] Dr. C. Platas-Iglesias
Dpto. Química Fundamental, Facultade de Ciencias
Universidade da Coruña, A Coruña (Spain)

[c] Prof. Dr. L. Vander Elst, Prof. Dr. R. N. Muller
NMR Laboratory, Department of Organic Chemistry
University of Mons-Hainaut, 7000 Mons (Belgium)

[d] Dr. W. Zhou
School of Chemistry, University of St Andrews
Haugh KY16 9ST, Fife (Scotland)

[e] Prof. Dr. C. F. G. C. Geraldes
Departamento de Bioquímica
Faculdade de Ciências e Tecnologia, e Centro de Neurociências
Universidade de Coimbra, Apartado 3126, 3049 Coimbra (Portugal)

  0947-6539/02/0822-5121 $ 20.00+.50/0

netriamine-*N*,*N*,*N*′,*N*′,*N*″-pentaacetate), [Gd(dtpa-bma)(H_2O)] (dtpa-bma = dtpa-bis(methylamide), [Gd(dota)(H_2O)]$^-$ (dota = 1,4,7,10-tetraazacyclododecane-1,4,7,10-tetraacetate) and [Gd(hp-do3a)(H_2O)] (hp-do3a = 10-(2-hydroxypropyl)1,4,7,10-tetraazacyclododecane-1,4,7-triacetate). The Gd^{3+} ion is especially suitable because of its high electron spin (S = 7/2) and relatively slow electronic relaxation. The evolution of the MRI technique has given rise to an increasing demand for contrast agents that target specific organs, regions of the body or diseased tissue. Examples of specific MRI contrast agents that have been developed up to now are MS-325[11–13] for cardiovascular imaging and Gadolite,[14–16] which is a Gd^{3+}-modified NaY zeolite for imaging of the gastrointestinal tract. More recently, Reynolds et al.[17] have reported Gd^{3+}-loaded nanoparticles with a diameter of 120 nm to be of potential use as a MRI contrast agent for both the gastrointestinal tract and the intravascular system, since the particles are small enough to pass through the vasculature. A new kind of fibrin-targeted, nanosized contrast agent was recently reported for diagnosis of human thrombus.[18] If one is to take a rational rather than a trial-and-error approach to design new diagnostics, a detailed knowledge of the mechanisms that produce relaxivity is required along with an understanding of how changes in the chemical structure of the drug interfere with these mechanisms. Although these mechanisms are well understood in the case of contrast agents in homogeneous solution, the mechanisms governing the relaxivity in aqueous suspensions of materials, such as zeolites, remain much less explored.

In this work we present a study of very small Gd^{3+}-loaded zeolite NaY nanoparticles, which have a relaxivity that is substantially higher than that of Gadolite, previously reported by Balkus et al.[14–15] Zeolite NaY is a microporous aluminosilicate based on sodalite cages (which can be seen as a truncated octahedron) that are joined by O bridges between the hexagonal faces. Eight such sodalite cages are linked leaving a large central cavity or supercage, with a diameter of 12.5 Å (see Figure 1). The supercages share a 12-membered ring with an open diameter of 7.4 Å. These nanosized Gd-NaY systems are of potential use as MRI contrast agents for the gastrointestinal tract and maybe even for the intravascular system. The nanoparticles have been fully characterised in the solid state and their relaxivity is described for samples with different Gd^{3+} loadings. A combination of two techniques, NMR dispersion (NMRD) and EPR spectroscopy, is used to determine the parameters that govern relaxivity in these systems, and a two-step model is presented to account for the transmission of the relaxivity from the paramagnetic centers in the zeolite cavities to the bulk water outside the zeolite.

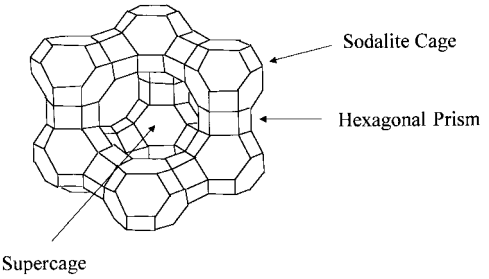

Figure 1. A representation of the framework of zeolite NaY.

Results and Discussion

Synthesis and characterisation of the exchanged zeolites: Nanosized Ln^{3+}-containing Y zeolites (Ln = La or Gd) were prepared by the exchange of NaY (mean diameter 80 nm) with $LnCl_3$ in water at pH 5.5. The amount of Ln^{3+} ions loaded into the NaY zeolite can be easily controlled by changing the NaY/Ln molar ratio during the synthesis (Table 1). From the elemental analyses, it can be calculated that the exchanged zeolites obtained contain 1.5 – 7.4 Gd^{3+} ions per unit cell, which corresponds to 0.2 – 0.9 Gd^{3+} per supercage. It can also be calculated that the charges of the aluminate units in these materials are not fully compensated by Ln^{3+} and Na^+. Most likely protons balance the remaining charge. The Si/Al ratio did not change substantially upon Ln^{3+} exchange (Table 1), which indicates that no dealumination occurred during the syntheses. High-resolution TEM (HRTEM) images of zeolite LaNaY-9.3 demonstrate that no substantial aggregation occurred during the synthesis of the exchanged nanoparticles. A typical particle of the exchanged zeolite is nonspherical with dimensions of 60 – 100 nm (Figure 2). The diffraction patterns of the GdNaY zeolites show that with increasing ion exchange, the intensity of individual reflections decreases, in agreement with previous observations on La^{3+}-exchanged NaY zeolites.[19] The zeolite XRD pattern shows a significant change of the integrated intensity of some reflections after Gd^{3+} or La^{3+} exchange. Similar changes have previously been observed for zeolites NaY upon extensive ion exchange with La^{3+} and Gd^{3+}.[15] The intensity of the 111 reflection dramat-

Table 1. Synthetic conditions and elemental analysis[a] data for the zeolites used in this work.

	NaY [g]	$LnCl_3 \cdot x\,H_2O$[b] [g]	Elemental analysis [%]					Si/Al	Crystal size [nm][e]
			Gd[c]	La[c]	Na[d]	Al[d]	Si[d]		
NaY					9.8	10.0	16.7	1.60	89
GdNaY-5.4	1.5	0.4178	5.4		2.4	9.0	15.0	1.60	72 – 74
GdNaY-5.0	1.5	0.3000	5.0		3.6	9.2	15.0	1.57	81 – 85
GdNaY-3.6	1.5	0.2000	3.6		4.4	9.7	19.0	1.88	90 – 92
GdNaY-2.3	1.5	0.1000	2.3		6.5	9.4	18.0	1.84	82 – 83
GdNaY-1.3	1.5	0.0500	1.3		7.7	10.1	19.0	1.81	94 – 104
La-2.8-GdNaY-3.3	1.5	0.2 (Gd)-0.2 (La)	3.3	2.8					80 – 82
LaNaY-9.3	2.0	0.5570		9.3	3.3	9.7	17.0	1.68	85 – 87

[a] All values are given in mass %. [b] La: x = 7; Gd: x = 6. [c] Neutron activation. [d] ICP. [e] Calculated from the Scherrer equation.

0947-6539/02/0822-5122 $ 20.00+.50/0 *Chem. Eur. J.* **2002**, *8*, No. 22

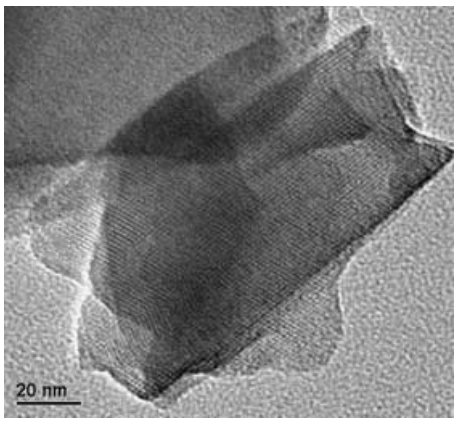

Figure 2. HRTEM picture of a typical LaNaY-9.3 nanoparticle.

ically decreases upon Ln^{3+} exchange, while the 222 reflection, which is not observed in the XRD pattern of the parent NaY, grows at the expense of the 311 reflection. Crystal sizes, as calculated by the Scherrer equation (see Table 1), are in good agreement with the TEM results for LaNaY-9.3.

The ion exchange of zeolite NaY with $LaCl_3 \cdot 7H_2O$ was monitored by ^{23}Na NMR spectroscopy on an aqueous suspension of the zeolite at pH 6.8 (Figure 3). The spectrum of NaY shows a broad resonance overlapped with a sharp ^{23}Na resonance, which we assign to Na^+ inside and outside the

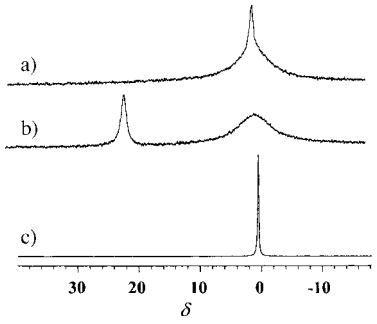

Figure 3. a) ^{23}Na NMR spectra of a NaY suspension in water at pH 6.8, b) the spectrum of this sample after addition of a small amount of $[Tm(dotp)]^{5-}$ and c) the spectrum after subsequent addition of excess $LaCl_3 \cdot 7H_2O$.

zeolite, respectively. The presence of Na^+ outside the zeolite indicates that protons replace some Na^+ ions when the zeolite is suspended in water at neutral pH; this is in agreement with observations made in the early days of zeolite research.[20] When the ^{23}Na shift reagent $[Tm(dotp)]^{5-}$ (H_8dotp = 1,4,7,10-tetraazacyclododecane-tetrakis-(methylenephosphonic acid)) was added to the sample of NaY, the peak corresponding to the Na^+ outside the zeolite shifted to higher frequency, while the resonance corresponding to the Na^+ inside the zeolite remained at the same position. This can be explained by the kinetic diameter of $[Tm(dotp)]^{5-}$, which is too large to allow the shift reagent to pass through the pores of the zeolite. Upon addition of an excess of $LaCl_3 \cdot 7H_2O$, the resonance for the inner Na^+ disappeared immediately; this indicates that La^{3+} very rapidly exchanges with the Na^+/H^+ cations that balance the negative charges inside the zeolite. After the addition of $LaCl_3 \cdot 7H_2O$, the peak for Na^+ outside the cavity shifted back to its original position at $\delta = 0$, because the La^{3+} ion interacts strongly with $[Tm(dotp)]^{5-}$, which "quenches" the shift reagent.

The chemical properties and the ionic radius of Y^{3+} (0.89 Å) are comparable to those of the Ln^{3+} ions (1.06–0.85 Å), and thus Y^{3+} complexes have coordination numbers and geometries that are closely related to those of the Ln^{3+} complexes. The exchange of $YCl_3 \cdot 6H_2O$ with zeolite NaY nanoparticles was studied by means of ^{89}Y NMR spectroscopy in D_2O suspensions of the NaY zeolite at pD 6.0. The ^{89}Y NMR spectrum of a $YCl_3 \cdot 6H_2O$/NaY mixture (1:3.5 w/w) displays two resonances at $\delta = -1$, a sharp one superimposed on a broad one. We assign these resonances to Y^{3+} ions outside and inside the zeolite, respectively. When a small amount of $[Tm(dotp)]^{5-}$ was added to the suspension, the peak from the Y^{3+} ions outside the zeolite shifts to high frequency, whereas the resonance of the Y^{3+} ions inside the zeolite remained at $\delta = -1$. This experiment confirms that the ^{89}Y peaks of $Y^{3+}(aq)$ ions inside and outside the zeolite have about the same chemical shifts, which points to similar coordination of Y^{3+} in both situations.

^{29}Si, ^{27}Al and ^{23}Na MAS NMR spectra: The ^{27}Al MAS NMR spectrum of LaNaY-9.3 exhibits a single sharp peak at $\delta = 60.3$ that is assigned to tetrahedrally co-ordinated Al^{3+} in the zeolitic framework, which is charge-balanced by La^{3+}, H^+ or Na^+ ions.[21] The spectra do not show any resonance around $\delta = 0$, which is the expected position for peaks corresponding to octahedral Al^{3+}. Since the presence of octahedral Al^{3+} generally indicates dealumination of the framework, this confirms that no dealumination occurred during the exchange process; this is also in agreement with the elemental analysis data (Table 1). Furthermore, the spectrum does not show the broad resonance at $\delta = 40-50$, which is usually assigned to tetrahedrally co-ordinated Al^{3+} in a distorted framework in calcined La(x)NaY zeolites.[22] This is probably caused by La^{3+} ions migrating to the most stable co-ordination positions in the sodalite cages upon calcination, while in uncalcined hydrated LaNaY-9.3 they are located in the supercages. This is consistent with previous studies of hydrated Ce-containing faujasites that place the rare-earth cation in the 12-membered ring of the supercages.[23, 24]

The ^{29}Si MAS NMR spectrum of LaNaY-9.3 has four maxima at $\delta = -91.9$, -96.0, -101.1 and -106.2 that are assigned to Si atoms bound to n $-O-Al\equiv$ groups and $4-n$ $-O-Si\equiv$ groups ($1 \le n \le 4$). The spectrum also shows a shoulder in the low frequency side that is assigned to Si atoms bound to four $-O-Si\equiv$ groups ($n = 0$, Figure 4). Each substitution of an $-O-Si\equiv$ by an $-O-Al\equiv$ results in a deshielding effect of ≈ 5 ppm. This is in agreement with previous observations on La^{3+}-exchanged Y zeolites with a Si/Al ratio of 2.6.[22] The spectrum of LaNaY-9.3 changes slightly with respect to that of the parent NaY zeolite: peaks slightly shift to lower frequency upon exchanging, and each of them seems to have one or more shoulders. This is probably because the La^{3+} cations are not mobile in the pores of the zeolite because of the strong electrostatic interaction with the zeolitic framework. Hence, only Si atoms in the vicinity of the La^{3+} ions feel

  0947-6539/02/0822-5123 $ 20.00+.50/0

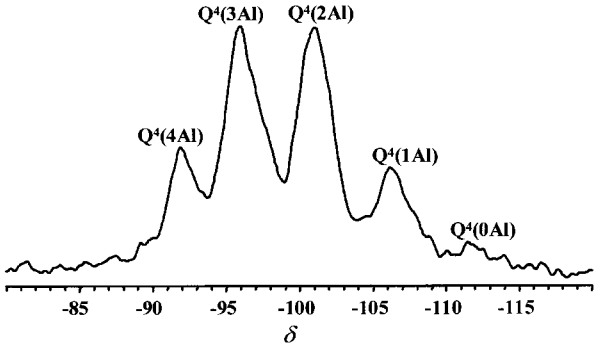

Figure 4. ^{29}Si MAS NMR spectrum of the LaNaY-9.3 sample. $Q^4(n\,Al)$ represents a Si atom bound to n −O−Al≡ groups and $4-n$ −O−Si≡ groups ($0 \le n \le 4$).

their presence and undergo a shift, the resulting spectrum being, in fact, a superimposition of several spectra.

The intensities of the five groups of peaks in NaY and LaNaY-9.3 can be used to calculate the overall Si/Al ratio of the framework. By applying Loewenstein's Rule,[25] which states that two tetrahedrally coordinated Al atoms on neighbouring T positions are avoided, Equation (1) can be used.[22]

$$\frac{\mathrm{Si}}{\mathrm{Al}} = \frac{\sum_{n=0}^{4} I_n}{\sum_{n=0}^{4} (n/4) I_n} \qquad (1)$$

In Equation (1) I_n is the intensity of the peak associated with a Si atom bound to n −O−Al≡ groups and $4-n$ −O−Si≡ groups ($0 \le n \le 3$). The Si/Al ratios determined by this method are 1.85 (NaY) and 1.66 (LaNaY-9.3), in good agreement with the elemental analysis data (Table 1). The smallest peak used while deconvoluting the spectra to determine the intensities was about 3–4 times the noise level. Taking this source of error into consideration, it can be concluded that no significant change in the Si/Al ratio occurs during La^{3+} exchange.

The ^{23}Na MAS NMR spectra of both LaNaY-9.3 and the starting NaY zeolite display a single resonance at $\delta = -2.4$ with linewidths of 381 and 403 Hz, respectively. This suggests that the exchange of Na^+ ions between the different cation sites in fully hydrated LaNaY is rapid on the NMR timescale at room temperature. This contrasts with previously reported studies of dehydrated NaY[26] and CsNaY[27] zeolites, for which different peaks for the different cation sites of the zeolite were observed.

EPR measurements: The X-band first-derivative EPR spectra of Gd^{3+} in the GdNaY zeolite samples with increasing Gd^{3+} content (Figure 5) are similar to those obtained previously for that zeolite containing hydrated Gd^{3+}, but differ from those observed upon calcination.[28–30] Similar spectra have also been observed for *S*-state ions, Gd^{3+} and Eu^{2+}, when present at low concentrations in glassy hosts. It is known as the U spectrum, [28] because of its ubiquity in vitreous materials[31–42] and in disordered polycrystalline materials, such as zeolites[28–30] and PLZT ceramics.[43] It shows three prominent features with effective g values of $\approx$6.4, 2.6 and 2.0, ($g = h\nu/\mu_B H$, h is the Planck constant, ν is the microwave frequency, μ_B is the Bohr magneton and H is the value of the externally applied magnetic field at the position of the resonance line), with an additional low-intensity feature at very low field ($g \approx$ 8.4), superimposed on a broad resonance lineshape that encompasses the $g \approx 2.0$ feature. Several qualitative and contradictory interpretations of this EPR spectrum have been proposed that used different multiple-site models with distinct types of rhombic crystal field (CF) parameter strengths and asymmetries.[35, 36, 43, 44] Only a quantitative fitting of the experimental spectra,[45] based on an ab initio computer simulation, with explicitly incorporated broad distributions in the CF parameters, led to a comprehensive interpretation of the EPR spectrum.[46] The assumption regarding the CF parameters was confirmed by results of optical absorption and fluorescence studies of Eu^{3+} in glasses and Y zeolite.[47, 48] Thus, a general solution of the U-type EPR spectrum consists of a convolution of a broad distribution of second-order CF parameters, b_2^0, with a maximum in the range $0.051\ \mathrm{cm}^{-1} \le b_2^0 \le 0.056\ \mathrm{cm}^{-1}$, and a broad distribution of asymmetry parameters, $\lambda' = b_2^2/b_2^0$, with appreciable probability over the whole range $0.0 \le \lambda' \le 1.0$.[46] The site symmetries of the Ln^{3+} ions are essentially very low and disordered, ranging from axial to rhombic, and are best characterised by a single low-symmetry "glassy type" site. Thus, the prominent features of the EPR spectrum at $g \approx 6.4$ and 2.6 are identified with specific EPR transitions that are stationary with respect to b_2^0, λ' and the orientation angles of the applied field H over a wide range, and are not associated with a small number of distinct or preferentially occupied sites for the Ln^{3+} ions, as previously proposed.[35, 36, 43, 44] The broad $g \approx 2.0$ feature can be attributed almost entirely to isolated Ln^{3+} ions, with some contribution from clustered ions.

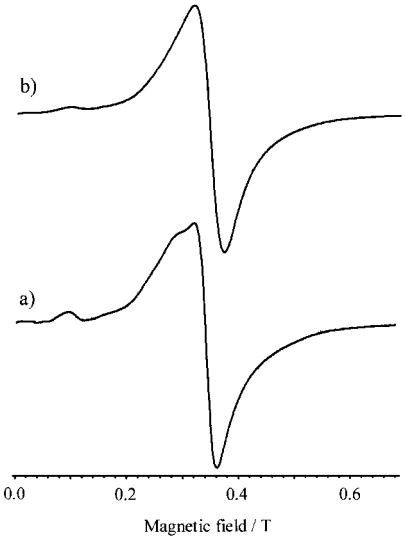

Figure 5. EPR spectra (X band, 0.34 T, 9.43 GHz) of solid GdNaY zeolite samples at 298 K as a function of the Gd^{3+} content: a) 1.3 wt % Gd; b) 5.4 wt % Gd.

For the GdNaY zeolite samples studied in this work, at 298 K an increase of the Gd^{3+} content increases the intensity of the EPR feature at $g \approx 2.0$ relative to the $g \approx 6.4$, $g \approx 2.6$ and $g \approx 8.4$ features, becoming predominant for the sample with

0947-6539/02/0822-5124 $ 20.00+.50/0 *Chem. Eur. J.* **2002**, *8*, No. 22

5.4 wt % Gd (data not shown). The linewidths of all signals increase with increasing Gd^{3+} content, in particular that of the $g \approx 2.0$ signal, as a result of dipole–dipole broadening. Such a dependence of EPR line intensities and widths on Gd^{3+} content has also been observed for borate glasses containing Gd^{3+}.[35, 37, 39, 41, 42] Studies of the temperature dependence of the magnetic susceptibility of these glasses as a function of Gd^{3+} content[41, 42] show evidence of weak antiferromagnetic interactions between Gd^{3+} ions generating a considerable number of Gd-O-Gd dimers that coexist with isolated Gd^{3+} ions. This correlates with the relative prominence of the $g \approx 2.0$ signal at high Gd^{3+} content, which can have some contribution from clustered Gd^{3+} ions. It is also confirmed by our observation that the 77 K EPR spectrum of the 5.4 % Gd sample shows a substantial increased intensity of the $g \approx 2.6$ and $g \approx 6.4$ signals relative to $g \approx 2.0$ (data not shown).

The X-band EPR spectra of the various GdNaY zeolite nanoparticles were also studied in aqueous suspensions at 298 K (data not shown). In contrast to the spectra obtained in the solid state, they display a single, approximately Lorentzian resonance with $g \approx 2.0$,[16] probably resulting from rotational averaging of the various anisotropic magnetic interactions present (g tensor, hyperfine tensor and zero-field splitting tensor). The transverse electronic relaxation rates, $1/T_{2e}$, were calculated from the peak-to-peak EPR line widths, ΔH_{pp}, with Equation (2), in which the symbols have their usual meaning.[49]

$$\frac{1}{T_{2e}} = \frac{g_L \mu_B \pi \sqrt{3}}{h} \Delta H_{pp} \qquad (2)$$

For the zeolite GdNaY nanoparticles studied the linewidths, and hence the relaxation rates, increased with increasing Gd^{3+} loading (Table 2).

Proton relaxation (NMRD) in aqueous suspensions: The ability of Gd^{3+} complexes to enhance the nuclear relaxation rate of solvent water protons is the result of the efficient dipolar magnetic coupling between the unpaired electrons of the Gd^{3+} ion and the nuclear spins. This process is believed to occur simultaneously following three different mechanisms:[1–4] 1) diffusion of water molecules in the proximity of the paramagnetic complex (outer-sphere contribution), 2) exchange of the water molecules from the co-ordination site to the bulk (inner-sphere contribution) and 3) prototropic exchange involving mobile protons of the complex or of the co-ordinated water itself. For water suspensions of Gd^{3+}-containing zeolites, Gd^{3+} inner-sphere water molecules must exchange with the water molecules located inside the zeolite cavities and then diffuse through the zeolite channels and exchange with the bulk to enable efficient propagation of the relaxation effect. To account for the relaxivity in aqueous suspensions of zeolites, we assumed a two-step model in which the interior of the zeolite is considered to contain a concentrated aqueous solution of Gd^{3+}, which exchanges with the bulk water outside the zeolite (Figure 6). A similar model has been applied previously to a qualitative interpretation of NMRD data.[16] We assume that the exchange between Gd^{3+}-bound water and the water inside the zeolite cavity is much faster than the exchange between water inside with that outside the zeolite. Thus, we can separate the two exchange processes concerned.

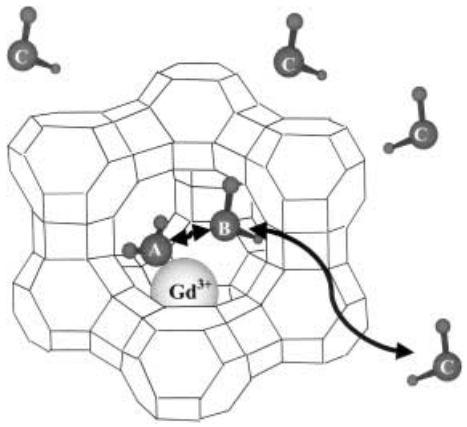

Figure 6. Schematic representation of the "two-step" model to account for the relaxivity in aqueous suspensions of Gd^{3+}-loaded zeolite Y; A represents a water molecule coordinated to Gd^{3+}, B an intra-framework water molecule not coordinated to Gd^{3+} and C bulk water molecules.

The outer-sphere contribution to the relaxivity is usually accounted for by the Freed model.[50] It arises from diffusing water molecules close to the paramagnetic centre, and it is inversely proportional to the diffusion coefficient of a water molecule away from the Gd^{3+} particle, (D_{GdH}), and the

Table 2. Parameters obtained from least-squares fits of NMRD and EPR data.

	GdNaY-5.4	GdNaY-5.0	GdNaY-3.6	GdNaY-2.3	GdNaY-1.3	La-2.8GdNaY-3.3
τ_R^{298} [s]				$> 1 \times 10^{-9}$[a]		
E_R [kJ mol^{-1}]				6 ± 2[a]		
τ_{zeo}^{298} [10^{-5} s]				3.3 ± 0.9[a]		
E_{zeo} [kJ mol^{-1}]				8.4 ± 0.2[a]		
E_v [kJ mol^{-1}]				6 ± 1[a]		
τ_v^{298} [ps]	25 ± 3	22 ± 2	22 ± 2	21.8 ± 0.6	24 ± 1	26 ± 1
Δ^2 [10^{19} s^{-2}]	5.6 ± 0.2	5.1 ± 0.1	4.4 ± 0.1	4.02 ± 0.04	3.84 ± 0.04	3.90 ± 0.05
τ_m^{298} [ns]	769 ± 238	625 ± 156	10.0 ± 0.8	5.9 ± 0.3	4.0 ± 0.2	14.3 ± 0.8
E_m [kJ mol^{-1}]	57 ± 6	26 ± 5	12 ± 2	4 ± 1	1[b]	11 ± 2
x	11 ± 5	13 ± 1	22 ± 9	37 ± 13	60 ± 21	21 ± 2
$1/T_{2e}$ [10^7 s^{-1}][c]	779.54	678.38	597.35	536.63	526.53	546.66
$1/T_{2e}$ [10^7 s^{-1}][d]	779.56	678.40	597.37	536.65	526.53	546.70

[a] Parameters independent of Gd^{3+} loading. [b] Parameters fixed with the least-square procedure. [c] From EPR data at 298 K and a magnetic field strength of 0.34 T. [d] From simultaneous fit of NMRD and EPR at 298 K and a magnetic field strength of 0.34 T.

  0947-6539/02/0822-5125 $ 20.00+.50/0

distance of closest approach of an outer sphere water molecule to the Gd^{3+} centre (a_{GdH}). The value of a_{GdH} was estimated to be 3.5 Å for Gd^{3+} chelates in aqueous solutions.[51] We can safely assume this outer-sphere contribution to be negligible for water molecules outside the zeolite particle. Inside the zeolite cavity, however, unbound water molecules are able to diffuse close to the Gd^{3+} ion. The self-diffusion coefficient of water in NaY zeolites has been determined by NMR techniques,[52] and its value is of the same order of magnitude as those determined for water protons in homogeneous solutions of Gd^{3+} chelates. The NMRD profiles of the GdNaY samples show relatively high maxima at ≈60 MHz, which is characteristic for immobilised Gd^{3+} (see below). Simulations show that, under those conditions, the outer-sphere contribution to the overall relaxivity is small, particularly at Larmor frequencies higher than 0.1 Hz. Therefore, we also neglected the outer-sphere contribution from the water molecules inside the zeolite particles at this stage.

For both processes of our two-step model, we derive approximate equations from the exact solution of the Bloch equations for the longitudinal relaxation time of a system in which water protons undergo chemical exchange between two magnetically distinct environments A and B [Eq. (3)].[53–55]

$$\frac{1}{T_1}=A_1\pm\left[A_1^2-\left(\frac{1}{\tau_{1A}\tau_{1B}}-\frac{1}{\tau_a\tau_b}\right)\right]^{1/2},\ A_1=\frac{1}{2}\left[\frac{1}{\tau_{1A}}+\frac{1}{\tau_{1B}}\right],\ \frac{1}{\tau_{1A}}=\frac{1}{T_{1A}}+\frac{1}{\tau_a} \quad (3)$$

In Equation (3) T_{1A} is the intrinsic relaxation time in the A environment in the absence of exchange and τ_a is the residence time in the A environment. Analogous definitions apply for the B environment. Considering the B system as the water inside the zeolite cavities and the A system to constitute the bulk water and assuming that $T_{1A}\gg T_{1B}$ and $\tau_a\gg\tau_b$, the observed proton relaxivity in $s^{-1}mM^{-1}$ can be expressed by Equation (4):[54]

$$r_1=\frac{1}{1000}\frac{x+q}{55.5}\frac{1}{T_{1zeo}+\tau_{zeo}} \quad (4)$$

in which c is the Gd^{3+} "concentration" in $molL^{-1}$, x is the number of free water molecules inside the zeolite per Gd^{3+} ion (water molecules not coordinated to Gd^{3+}), q is the number of inner sphere water molecules coordinating to the Gd^{3+} ion, τ_{zeo} is the residence time of the water protons inside the zeolite and $1/T_{1zeo}$ is the relaxation rate of water protons inside the zeolite.

The inequality $\tau_a\gg\tau_b$ serves as an expression of the dilution of the B species, and therefore Equation (4) is only valid for dilute solutions of paramagnetic species. However, the condition $\tau_a\gg\tau_b$ does not necessarily hold for the interior of the zeolite, since the number of water molecules per Gd^{3+} ion can be relatively low, especially for high Gd^{3+} loadings. Therefore, to evaluate $1/T_{1zeo}$, we assume a chemical exchange between two magnetically distinct chemical environments in a concentrated system: water protons in the interior of the zeolite (A environment) and water molecules in the inner coordination sphere of the Gd^{3+} ion (B environment). The Taylor expansion to first order of the square root in Equation (3) gives Equation (5):

$$\left[A_1^2-\left(\frac{1}{\tau_{1A}\tau_{1B}}-\frac{1}{\tau_a\tau_b}\right)\right]^{1/2}\approx A_1-\frac{M}{2A_1},\ M=\frac{1}{\tau_{1A}\tau_{1B}}-\frac{1}{\tau_a\tau_b} \quad (5)$$

Substitution of this expression into Equation (3), taking the negative root, gives Equation (6):

$$\frac{1}{T_1}\approx\frac{M}{2A_1}=\frac{\left(\frac{1}{T_{1A}}+\frac{1}{\tau_a}\right)\left(\frac{1}{T_{1B}}+\frac{1}{\tau_b}\right)-\left(\frac{1}{\tau_a\tau_b}\right)}{\left(\frac{1}{T_{1A}}+\frac{1}{\tau_a}\right)+\left(\frac{1}{T_{1B}}+\frac{1}{\tau_b}\right)} \quad (6)$$

In the trivial case of absence of exchange ($1/\tau_a=1/\tau_b=0$), we simply obtain the two relaxation times of the A and B systems separately ($T_1=T_{1A}+T_{1B}$). To evaluate $1/T_{1zeo}$ we make the following approximation [Eq. (7)]:

$$\frac{1}{T_{1A}}\ll\frac{1}{\tau_a} \quad (7)$$

Then Equation (8) can be derived from Equation (6):

$$\frac{1}{T_1}=\frac{\tau_b}{\tau_a\tau_b+T_{1B}\tau_b+T_{1B}\tau_a} \quad (8)$$

The fraction of time that the nucleus spends in the A environment, f_A, is given by Equation (9):

$$f_A=\frac{\tau_a}{\tau_a+\tau_b} \quad (9)$$

with an analogous definition for f_B. A little algebra allows Equation (10) to be derived from Equations (8) and (9):

$$\frac{1}{T_1}=\frac{\frac{f_B}{f_A}}{\tau_b+T_{1B}\left(1+\frac{f_B}{f_A}\right)} \quad (10)$$

For convenience, Equation (10) may be written as Equation (11) to describe the longitudinal relaxation rate of water protons in the interior of a zeolite:

$$\frac{1}{T_{1zeo}}=\frac{\frac{q}{x}}{\tau_m+T_{1m}\left(1+\frac{q}{x}\right)} \quad (11)$$

in which T_{1m} is the longitudinal relaxation time of inner sphere water protons and τ_m is the mean residence time of water protons in the inner sphere. It may be noted that, for very dilute solutions (i.e. $q/x\ll1$), Equation (11) simplifies to an expression analogous to Equation (4).

The longitudinal relaxation rate of the inner-sphere water molecules is dominated by the dipolar interaction and is given by the Solomon–Bloembergen equation [Eq. (12)]:[56, 57]

$$\frac{1}{T_{1m}}=\frac{2}{15}\left(\frac{\mu_0}{4\pi}\right)^2\frac{\hbar^2\gamma_S^2\gamma_I^2}{r_{GdH}^6}S(S+1)\left(\frac{3\tau_{d1}}{1+\omega_I^2\tau_{d1}^2}+\frac{7\tau_{d2}}{1+\omega_S^2\tau_{d2}^2}\right) \quad (12)$$

in which r_{GdH} is the effective distance between the gadolinium electronic spin and the water protons, γ_S (γ_I) is the electron (proton) gyromagnetic ratio and τ_{di} is given by $\tau_{di}^{-1}=\tau_m^{-1}+\tau_R^{-1}+T_{ie}^{-1}(i=1,2)$. The rotational correlation time (τ_R) concerns the rotation of the Gd^{3+}–water proton vector.

The electronic relaxation rates ($1/T_{ie}$) were approximated with Equations (13) and (14):[58, 59]

0947-6539/02/0822-5126 $ 20.00+.50/0 Chem. Eur. J. 2002, 8, No. 22

$$\frac{1}{T_{1e}} = \tfrac{1}{25}\Delta^2\tau_v[4S(S+1)-3]\left(\frac{1}{1+\omega_S^2\tau_v^2}+\frac{4}{1+4\omega_S^2\tau_v^2}\right) \quad (13)$$

$$\frac{1}{T_{2e}} = \Delta^2\tau_v\left(\frac{5.26}{1+0.372\,\omega_S^2\tau_v^2}+\frac{7.18}{1+1.24\,\omega_S^2\tau_v^2}\right) \quad (14)$$

in which ω_S is the Larmor frequency, Δ^2 is the trace of the square of the ZFS tensor, and τ_v is the correlation time for the modulation of ZFS.

We assumed all correlation times τ_p to have a simple exponential temperature dependence [Eq. (15)] with a value τ_p^{298} at 298.15 K and activation energy E_p.

$$\tau_p = \tau_p^{298}\exp\left[\frac{E_p}{R}\left(\frac{1}{T}-\frac{1}{298.15}\right)\right] \quad (15)$$

The magnetic field dependence of longitudinal proton relaxation (NMRD profile) of the GdNaY-2.3 sample studied in this work was recorded at 310, 298, 288 and 278 K. For the five remaining Gd^{3+}-containing samples, the magnetic field dependence of longitudinal proton relaxation was recorded at 310 K, and its temperature dependence was monitored at 20 and 300 MHz. The curves obtained are included in Figure 7. The increase of the relaxivity at high magnetic field (>10 MHz), observed in the NMRD profiles for all the Gd^{3+} loadings, is indicative of a relatively long rotational correlation time τ_R, thereby confirming the immobilisation of the Gd^{3+} ions in the zeolite. The temperature dependence of the NMRD profiles usually gives a good indication of the parameter limiting the proton relaxivity. If the relaxivity at high field (>10 MHz) increases with increasing temperature, it is limited by slow water exchange, whereas in the opposite case, fast rotation is the limiting factor. For the GdNaY zeolites, the relaxivity increases upon increasing the temperature, which shows that proton relaxivity is dominated by the slow water exchange, and that the diffusion of water through the zeolite channels to the bulk is, therefore, the limiting factor. Figure 7 also shows that the relaxivity increases with decreasing Gd^{3+} loading, in agreement with previous observations for GdNaY zeolites with undefined particle size.[15]

Several factors could be responsible for the decrease of the relaxivity upon increasing the Gd^{3+} loading: 1) the Gd^{3+} ion might block the diffusion of water protons through the zeolite channels to the bulk, 2) a change of the water hydration number q with the Gd^{3+} loading and 3) an inhomogeneous distribution of Gd in the zeolite. For example, particles with a low Gd^{3+} loading might have a relatively high Gd^{3+} concentration near the surface. In such a case, the contribution from the Gd^{3+} ions near the surface would dominate, which would explain the relatively high relaxivity at low loadings. To check if any of the factors mentioned above is responsible for the decrease of the relaxivity if the Gd^{3+} loading is increased, we have prepared a zeolite exchanged with a mixture of Gd^{3+} and La^{3+}. The resulting zeolite contained 3.3 wt % Gd and 2.8 wt % La (Table 1). The relaxivity of the La-2.8-GdNaY-3.3 sample is about the same as that expected for a similar sample without La^{3+} (GdNaY-3.3) (Figure 7), which excludes any of the above-mentioned factors as being responsible for the decrease of the observed relaxivity with increasing Gd^{3+} loading. Therefore, this effect must be a consequence of the normal decrease on the $x + q$ term in the numerator of Equation (4), because the number of water molecules per Gd^{3+} ion in the interior of the zeolite decreases on increasing the Gd^{3+} loading.

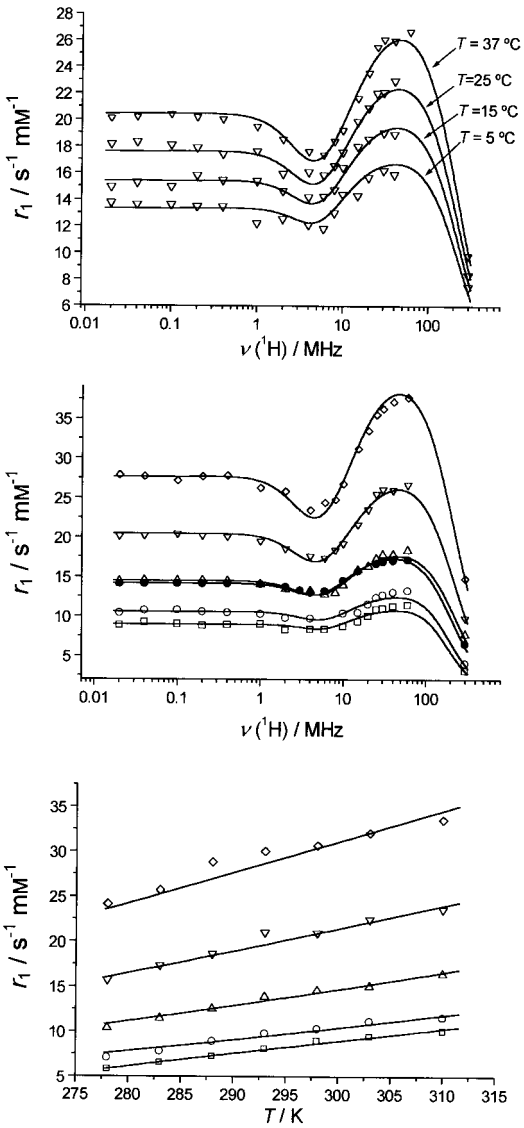

Figure 7. From top to bottom, NMRD profiles of GdNaY-2.3 recorded at different temperatures; NMRD profiles at different Gd^{3+} loadings for the GdNaY samples studied in this work at 37 °C and temperature dependence of the proton relaxivity at 20 MHz: GdNaY-1.3 (◇), GdNaY-2.3 (▽), GdNaY-3.6 (△), GdNaY-5.0 (○) and GdNaY-5.4 (□) and La-2.8-GdNaY-3.3 (●).

Simultaneous fitting of EPR and NMRD data: Since the NMRD profile obtained for the LaGdNaY sample indicates that both τ_R and τ_{zeo} do not change much with the Gd^{3+} loading, we performed a simultaneous fitting of the experimental data for the six samples studied in this work using the equations specified in the previous sections. The inner-sphere Gd^{3+}–H distance was fixed at 3.1 Å. The transversal electronic relaxation rates, as determined from the EPR spectra, were also included in the fitting procedure. We assumed that $q = 7$ for Gd^{3+} ions inside the supercages of hydrated zeolite Y. This assumption is supported by extended X-ray absorption fine structure (EXAFS) investigations on Eu^{3+}-exchanged

zeolite Y,[60] which demonstrated that one O atom of the framework is co-ordinated to Eu^{3+}. A q value of seven therefore results in an overall co-ordination number of eight for Gd^{3+}. Moreover, some of the parameters were assumed to be independent of the Gd^{3+} loading: τ_R, E_R, τ_{zeo}, E_{zeo} and E_v. In the case of τ_R and E_R, this is supported by independent fits of the NMRD data for each of the six samples studied. These fits show that, for each sample, the experimental data can be reproduced with any τ_R value above 1×10^{-9} s, since above this limit τ_R does not affect the relaxivity (vide infra). The same situation holds for E_v, the independent fittings for each sample giving very similar values (a few kJ mol^{-1}). The constancy of τ_{zeo} and E_{zeo} is supported by the comparison of the NMRD curves of La-2.8-GdNaY-3.3 and GdNaY-3.3, which shows that the diffusion of water molecules from the interior of the zeolite to the bulk is not blocked by the La^{3+} ions. We considered the parameters that describe the electronic relaxation (τ_v and Δ^2), as well as the parameters that describe the water exchange in the interior of the zeolite, (τ_m and x), as changing with the Gd^{3+} loading. An excellent fit of the experimental data points was obtained with this model by the use of the parameters listed in Table 2 (see also Figure 7).

Unfortunately, ^{17}O NMR spectroscopy, which is a technique widely used to obtain information on water exchange kinetics of MRI contrast agents in solution, appeared to be of little value in the study of aqueous suspensions of Gd-loaded NaY nanoparticles, since no ^{17}O $1/T_1$ or $1/T_2$ relaxation rate enhancement effects or paramagnetic induced shifts could be detected, most probably because the exchange of the water is slow on the ^{17}O NMR timescale (see below). As q has not been determined independently, we also performed fits of the experimental data by the use of lower q values. Although the quality of the fittings obtained was good assuming $q = 6$, we obtained an unreasonable x value for GdNaY-5.4 (≈ 1). Therefore, it appears that the present model can not account for the experimental data assuming q values lower than 7.

The $1/T_{2e}$ values calculated from the NMRD curves at 298 K are in excellent agreement with the experimental values obtained from the EPR peak-to-peak linewidths, which shows that the model can describe the electronic relaxation adequately. This gives us some confidence that neglecting the outer-sphere contribution to the relaxivity is justified. If this assumption were incorrect, this would most likely be compensated by T_{2e} during the fitting procedure.

The value of the Δ^2 parameter (which governs the ZFS mechanism of electronic relaxation) increases from 0.38×10^{20} s^{-2} at 1.3 wt % Gd to 0.56×10^{20} s^{-2} at 5.4 wt % Gd. The first of these values compares well with those obtained (through the magnetic field dependence of effective g values) for the quite symmetric aqueous monomeric species, such as $Gd^{3+}_{(aq)}$ ($\Delta^2 = 0.22 \times 10^{20}$ s^{-2}) and $[Gd(dota)(H_2O)]^-$ ($\Delta^2 = 0.124 \times 10^{20}$ s^{-2}), and the last is similar to that obtained for the almost rhombic $[Gd(dtpa)(H_2O)]^{2-}$ ($\Delta^2 = 0.7 \times 10^{20}$ s^{-2}).[61] This suggests that an interaction between neighbouring Gd^{3+} ions within the same particle, a higher Gd^{3+} content could produce a significant electronic relaxation effect, as previously demonstrated with dimeric Gd^{3+} chelates.[62] The parameter τ_v^{298} also governs the zero-field splitting mechanism of the electronic relaxation. Its value, as obtained from the fitting, seems to be almost independent of the Gd^{3+} loading and is close to those reported for $[Gd(dtpa)(H_2O)]^{2-}$ and $[Gd(dtpa\text{-}bma)(H_2O)]$, but larger than that reported for $Gd^{3+}_{(aq)}$ (7.3 ps).[51]

The τ_m^{298} values for the water exchange process in the zeolite supercages increase substantially upon increasing the Gd^{3+} loading, ranging between 769 ns for GdNaY-5.4 to 4 ns for GdNaY-1.3. The latter value is within an order of magnitude of the residence time of inner-sphere water molecules determined for $Gd^{3+}_{(aq)}$ ($\tau_m^{298} = 1.2$ ns).[51] The increase in the τ_m^{298} values with increasing Gd^{3+} loading is a consequence of the increase of the Gd^{3+} concentration inside the zeolite cavities, which makes the probability of a water molecule being located in the inner coordination sphere of the Gd^{3+} ion higher. This increasing concentration is also reflected in the number of water molecules per Gd^{3+} ion in the interior of the zeolite, with x values ranging from 11 ± 5 for GdNaY-5.4 to 60 ± 21 for GdNaY-1.3. This increase of the x values is also the main reason for the decrease of the observed relaxivity on increasing the Gd^{3+} loading as a result of the presence of the $x + q$ term in the numerator of Equation (4). From the values of x, it can be calculated that the amount of water inside the zeolite that is in exchange corresponds to 10–12 % of the weight of the zeolite, almost independent of the Gd^{3+} loading. The total amount of water in the zeolite amounts to ≈ 30 wt % of the zeolite. Therefore, it can be concluded that not all water inside the zeolite contributes to the exchange with the bulk water outside the zeolite. In previous literature, it has been reported that the water exchange between the supercage and the sodalite cages is very slow (1 mol in 4 days at 295 K)[63] and, therefore, the water molecules in the sodalite cages do not contribute to the propagation of the relaxivity. Furthermore, it is likely that the overall relaxivity is dominated by the contributions because of the exchange of water in the supercages closest to the particle surface with that outside the zeolite. Migration of Gd^{3+} from the supercages to the β cages can be excluded, since for such a migration to occur the hydrated zeolite has to be heated at temperatures close to 200 °C.[60]

The residence time of water protons in the interior of the zeolite is relatively long, but still short enough to allow an efficient propagation of the paramagnetically induced relaxation effect from the interior of the zeolite to the bulk water (τ_{zeo}^{298} is typically 110–115 times longer than τ_m^{298} observed for commercial MRI contrast agents).

The ^{17}O chemical shift of each of the seven Gd^{3+}-bound water molecules can be estimated (with respect to that of a free water molecule, $\Delta\omega$) to be about -6.34×10^5 rad s^{-1} at 7.05 T and 298 K.[1, 3] Assuming that the supercages are occupied by about 30 water molecules, the "averaged" $\Delta\omega$ value for the water molecules in the supercage can be estimated to be $\approx -1.5 \times 10^5$ rad s^{-1}. The absolute value is larger than $1/\tau_{zeo}$ (3×10^4 s^{-1}) and, therefore, the exchange of water between the supercages and the bulk is slow on the ^{17}O chemical shift timescale. Most likely, the ^{17}O resonance for water in the supercage is extremely broad and, therefore, escapes observation. Consequently, no paramagnetic effects could be observed in the ^{17}O NMR spectra of suspensions of

0947-6539/02/0822-5128 $ 20.00+.50/0 *Chem. Eur. J.* **2002**, *8*, No. 22

GdNaY. The chemical shifts of ^{1}H nuclei of Gd^{3+}-bound water molecules are considerably smaller than those of the ^{17}O nuclei. Therefore, it may be expected that the exchange is rapid on the ^{1}H NMR timescale, as is confirmed by the linear dependence of the relaxation rate enhancements on the amount of added GdNaY.

A relaxivity of $\approx 12\ s^{-1}\,mM^{-1}$ (40 MHz, room temperature) was reported for a GdNaY sample of undefined particle size and Si/Al ratio with a 2.3% Gd^{3+} loading.[16] The relaxivity obtained in the present study for a nanosized GdNaY-2.3 zeolite at 25 °C and 40 MHz amounts to $23\ s^{-1}\,mM^{-1}$, and the observed relaxivity for a sample with 1.3% loading at 40 MHz and 37 °C is as high as $37.2\ s^{-1}\,mM^{-1}$. The higher relaxivities obtained in the present study may be ascribed to a smaller particle size that would result in a shorter residence time inside the zeolite because of the shorter "pathway" for the protons to reach the bulk. Alternatively, it could be rationalised by a difference in Si/Al ratio. This parameter could also influence the relaxivity, since it affects the hydrophilicity of the material, which on its turn most likely affects the residence time of water inside the zeolite (τ_{zeo}).

The rotational correlation time, τ_R^{298}, calculated from the fittings of the NMRD curves ($> 1 \times 10^{-9}$ s) is at least 25 times longer than that for $Gd^{3+}_{(aq)}$ at 298 K (41 ps);[51] this indicates that the rotation of inner-sphere water molecules is considerably hindered by the anchoring of the Gd^{3+} ions inside the zeolite to the framework. A simulation of the relaxivity of GdNaY-1.3 as a function of τ_{zeo} and τ_R (Figure 8) shows that

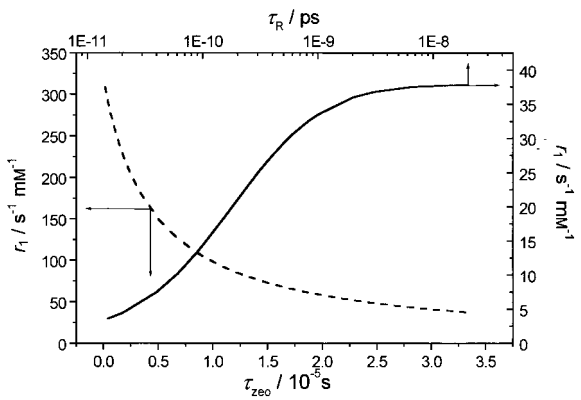

Figure 8. Simulation of the relaxivity at 37 °C for sample GdNaY-1.3 with the parameters reported in Table 2 as a function of τ_R and τ_{zeo}.

while the rotational correlation time for the GdNaY nanoparticles is in the optimum range, the water exchange between the zeolite supercages and the bulk is still far from the optimum value. The simulation shows that relaxivities as high as $310\ s^{-1}\,mM^{-1}$ could be achieved if one were able to immobilise Gd^{3+} with an optimum water exchange rate.

Conclusion

The results reported in this paper show that Gd^{3+}-containing NaY nanoparticles with a mean size of 80–100 nm display a very high relaxivity in aqueous suspensions. The experimental NMRD curves and EPR spectra can be explained by a two-step model that is based on the assumption that the interior of the zeolite contains a concentrated solution exchanging with the bulk water. This model requires the use of new equations, which we derived from the classical theory of exchange. Our results indicate that the Gd^{3+} ions are immobilised effectively in the interior of the zeolite cavities, which is reflected in a very long τ_R^{298}. The relaxivity is mainly limited by a relatively slow diffusion of water protons from the interior of the zeolite cavities to the bulk water. The decrease of relaxivity observed upon increasing the Gd^{3+} loading is mainly caused by a decrease in the number of water molecules per Gd^{3+} ion available in the zeolite cavities. Only the water molecules inside the large cages contribute to the exchange with the bulk water. The water exchange rate at 298 K on Gd^{3+} located in the zeolite supercages is within an order of magnitude of that on Gd^{3+}_{aq} in solution, but decreases drastically when the Gd^{3+} loading is increased.

In order to design new porous materials that display high relaxivities for application as contrast agents in MRI, some key features must be taken into account: 1) the material should be able to retain Gd^{3+} ions inside the framework with as many inner-sphere water molecules as possible, 2) the Gd^{3+} ion must be strongly coordinated to the framework to ensure a long τ_R and 3) the pores must be big enough to allow water molecules to diffuse from the interior of the material to the bulk water. Small particles containing big pores are expected to allow a more efficient water exchange rate. We believe that the approach used here may also be useful to describe the relaxivity in suspensions of other materials, such as other zeolites, clays or mesoporous materials, and liposomes. This will allow a more rational design of new potential contrast agents of these types. The formulation of a MRI contrast agent should contain the minimum amount of material that provides the maximum signal enhancement. Although the relaxivity of the Gd^{3+}-loaded NaY zeolites (expressed in $s^{-1}\,mM^{-1}\,Gd^{3+}$) decreases with the loading, the optimal relaxation rate enhancement expressed in $s^{-1}\,g^{-1}$ at 60 MHz is reached at a Gd^{3+} loading of 4.0–5.0 wt%.

Experimental Section

Materials: The batch of zeolite NaY used in this study was a gift from Akzo Nobel. Lanthanide chlorides ($LnCl_3 \cdot x\,H_2O$, $x = 7$, Ln = La; $x = 6$, Gd) and xanthan gum were purchased from Aldrich. ^{17}O-Enriched water (10% labelling) was purchased from Cortec (Paris, France).

Physical methods: X-ray powder diffraction (XRD) patterns were obtained with a D-5000 Siemens X-ray diffractometer, with nickel-filtered $Cu_{K\alpha}$ radiation ($\lambda = 1.5406$ Å). The samples were scanned in the 2θ range of 5–50° with steps of 0.015°. All crystal sizes were calculated from the line broadening (full width at half-height) of the [331], [511] and [440] reflections by using the Scherrer equation[64] and assuming that the broadening exclusively originates from size effects. High-resolution transmission electron microscopy (HRTEM) was performed on a Jeol JEM-2010 electron microscope operated at 200 kV. Elemental analyses were carried out with ICP-OES by dissolving the samples in a 1% HF/1.3% H_2SO_4 mixture. All the samples were measured twice as an independent duplicate. Neutron diffraction analyses were carried out on a ROG neutron reflectometer. ^{1}H (300 MHz), ^{23}Na (79.353 MHz) and ^{17}O (40.7 MHz) NMR spectra were recorded on a Varian INOVA-300 spectrometer in 5 mm sample tubes. The very high stability of the magnet made a field-

frequency lock unnecessary. ^{89}Y (19.596 MHz) NMR spectra were recorded on a Varian VXR-400S spectrometer in 5 mm sample tubes. The ^{23}Na, ^{17}O and ^{89}Y chemical shifts were measured with respect to external 0.1M NaCl in D_2O, D_2O and 0.1M YCl_3 in D_2O, respectively (substitution method). The $1/T_1$ nuclear magnetic resonance dispersion (NMRD) profiles were recorded at 5, 15, 25 and 37 °C with a field cycling system covering a range of magnetic fields from 2.5×10^{-4} to 1.2 T (corresponding to a proton Larmor frequency range of 0.01 – 50 MHz). The relaxivities at 300 MHz were determined with a Varian INOVA-300 spectrometer. The pH of the samples was measured at ambient temperature by means of a Corning 125 pH meter with a calibrated microcombination probe purchased from Aldrich. MAS ^{29}Si, ^{27}Al and ^{23}Na MAS NMR spectra were recorded on a Varian VXR-400S spectrometer with resonance frequencies of 79.460 (^{29}Si), 104.229 (^{27}Al) and 105.805 (^{23}Na) MHz. The spectrometer was equipped with a DOTY probe and 5 mm rotors with magic angle spinning at 4.5 kHz. The EPR spectra were recorded on a Bruker ESP300E Spectrometer, operating at 9.43 GHz (0.34 T, X-band), at 298 K and 77 K. EPR spectra of solid samples were obtained in Wilmad quartz tubes and aqueous suspensions in a quartz flat cell. Typical parameters used were: microwave power 4 mW, modulation amplitude 1.0 mT and time constant 0.03 s. The frequency was calibrated with diphenylpicrylhydrazyl (dpph) and the magnetic field with Mn^{2+} in MgO.

Sample preparation: All suspensions were prepared by weight. Samples for NMRD were prepared by suspending ≈10 mg of the concerning solid GdNaY zeolite in doubly distilled water (9 mL) containing 0.2% of xanthan gum as a surfactant. The suspensions were dispersed in an ultrasonic bath for 5 min. Measurements were performed on 600 µL aliquots of the former suspensions. The pH of the suspensions was 7.5.

Calculations: Experimental variable-temperature NMRD and EPR data were fitted with a modified version of a computer program written by É. Tóth and L. Helm (EPFL Lausanne, Switzerland) using the Micromath Scientist program version 2.0 (Salt Lake City, UT, USA).

Preparation of LnNaY (Ln = La or Gd): Zeolite NaY was stirred in an aqueous 1M NaCl solution at room temperature overnight, then centrifuged and washed with deionised water. The suspension was centrifuged again and the procedure was repeated until the water was free of chloride ($AgNO_3$ test). The pre-treated zeolite (1.5 g) was suspended in deionised water (10 mL). The pH of the suspension obtained was adjusted to 5.5 with 0.1M HCl. The required amount of $LnCl_3 \cdot 6H_2O$ was added to the mixture (see Table 1) and the resultant slurry was stirred overnight at room temperature. The suspension was then dialysed against water (cellulose tubing, Sigma, 12 KD cut-off) for 24 h, and the water removed under reduced pressure at room temperature.

Acknowledgements

We gratefully acknowledge the help of Dr. Zhiping Shan for recording the XRD patterns, Peter Boeser for performing the neutron activation analysis of the samples, Corinne Piérart for recording the NMRD profiles, and Prof. J. Reedijk (University of Leiden, The Netherlands) and his co-workers for assistance with some initial EPR experiments. This research was performed within the framework of the EU COST Action "Lanthanide Chemistry for diagnosis and therapy" (D18).

[1] *The Chemistry of Contrast Agents in Medical Magnetic Resonance Imaging* (Eds.: A. E. Merbach, É. Tóth), Wiley, Chichester, England, **2001**.
[2] P. Caravan, J. J. Ellison, T. J. McMurry, R. B. Lauffer, *Chem. Rev.* **1999**, *99*, 2293.
[3] J. A. Peters, J. Huskens, D. J. Raber, *Prog. Magn. Reson. Spectrosc.* **1996**, *28*, 283.
[4] S. M. Rocklage, A. D. Watson, M. J. Carvlin, *Magnetic Resonance Imaging*, 2nd ed., Mosby Year Book, St Louis, MO, **1992**, Chapter 14.
[5] P. Rongved, T. H. Fritzell, P. Strande, J. Klaveness, *Carbohydr. Res.* **1996**, *287*, 77.
[6] D. M. Corsi, L. Vander Elst, R. N. Muller, H. van Bekkum, J. A. Peters, *Chem. Eur. J.* **2001**, *7*, 64.
[7] N. Fatin-Rouge, É. Tóth, D. Perret, R. H. Backer, A. E. Merbach, J.-C. G. Bünzli, *J. Am. Chem. Soc.* **2000**, *122*, 10810.
[8] J. P. André, É. Tóth, H. Fisher, A. Seelig, H. R. Mäcke, A. E. Merbach, *Chem. Eur. J.* **1999**, *5*, 2977.
[9] S. Aime, A. Botta, M. Fasano, S. Geminatti Crich, E. Terreno, *Coord. Chem. Rev.* **1999**, *185/186*, 312.
[10] S. Aime, E. Gianolio, E. Terreno, G. B. Giovenzana, R. Pagliarin, M. Sisti, G. Palmisano, M. Botta, M. P. Lowe, D. Parker, *J. Biol. Inorg. Chem.* **2000**, *5*, 488.
[11] T. J. McMurry, H. Sajiki, D. M. Scott, R. B. Lauffer, WO 9623526 A2, **1996**.
[12] D. J. Parmelee, R. Walovitch, H. S. Ouellet, R. B. Lauffer, *Invest. Radiol.* **1997**, *32*, 741.
[13] R. N. Muller, B. Radüchel, S. Laurent, J. Platzek, C. Piérart, P. Mareski, L. Vander Elst, *Eur. J. Inorg. Chem.* **1999**, 1949.
[14] K. J. Balkus, Jr., A. D. Sherry, S. W. Young, *US Patent* 5122363 A, **1992**.
[15] I. Bresinska, K. J. Balkus, Jr., *J. Phys. Chem.* **1994**, *98*, 12989.
[16] S. K. Sur, J. F. Heinsbergen, R. G. Bryant, *J. Magn. Reson. A* **1993**, *103*, 27.
[17] C. H. Reynolds, N. Annan, K. Beshah, J. H. Huber, S. H. Shaber, R. E. Lenkinski, J. A. Wortman, *J. Am. Chem. Soc.* **2000**, *122*, 8940.
[18] X. Yu, S.-K. Song, J. Chen, M. J. Scott, R. J. Fuhrhop, C. S. Hall, P. J. Gaffney, S. A. Wickline, G. M. Lanza, *Magn. Reson. Med.* **2000**, *44*, 867.
[19] Z. Sarbak, *Catalysis Today* **2001**, *65*, 293.
[20] D. W. Breck, W. G. Eversole, R. M. Milton, T. B. Reed, T. L. Thomas, *J. Am. Chem. Soc.* **1956**, *78*, 5963.
[21] B. H. Wouters, T. Chen, P. Grobet, *J. Phys. Chem. B* **2001**, *105*, 1135.
[22] J. A. van Bokhoven, A. L. Roest, D. C. Koningsberger, J. T. Miller, G. H. Nachtegaal, A. P. M. Kentgens, *J. Phys. Chem. B* **2000**, *104*, 6743.
[23] D. H. Olson, G. T. Kokotailo, J. F. Charnell, *Nature* **1967**, *215*, 270.
[24] D. H. Olson, G. T. Kokotailo, J. F. Charnell, *J. Colloid Interface Sci.* **1968**, *28*, 305.
[25] W. Loewenstein, *Am. Mineral.* **1954**, *39*, 92.
[26] K. H. Lim, C. P. Grey, *J. Am. Chem. Soc.* **2000**, *122*, 9768.
[27] M. Hunger, U. Schenk, A. Buchholz, *J. Phys. Chem. B* **2000**, *104*, 12230.
[28] L. E. Iton, J. Turkevitch, *J. Phys. Chem.* **1977**, *81*, 435.
[29] L. E. Iton, S. L. Suib, G. D. Stucky, *Bull. Magn. Reson.* **1981**, *2*, 174.
[30] L. E. Iton, C. M. Brodbeck, S. L. Suib, G. D. Stucky, *J. Chem. Phys.* **1983**, *79*, 1185.
[31] N. S. Garif'yanov, R. K. Timerov, N. F. Usacheva, *Sov. Phys. Solid State* **1962**, *4*, 2448.
[32] G. G. Mshvelidze, K. I. Gapringashvili, *Sov. Phys. Solid State* **1972**, *13*, 2860.
[33] G. O. Karapetyan, D. M. Yudin, D. G. Gallimov, *Bull. Acad. Sci. USSR Phys. Ser.* **1967**, *31*, 814.
[34] I. V. Chepeleva, V. N. Lazulin, S. A. Dembovskii, *Sov. Phys. Dokl.* **1967**, *11*, 864.
[35] R. C. Nicklin, J. K. Johnstone, R. G. Barnes, D. R. Wilder, *J. Chem. Phys.* **1973**, *59*, 1652.
[36] L. Čugonov, J. Kliava, *J. Phys. C* **1982**, *15*, L933.
[37] S. K. Mendiratta, L. C. Costa, E. G. de Sousa, *J. Mater. Sci. Lett.* **1990**, *9*, 301.
[38] M. A. Valente, S. K. Mendiratta, *Phys. Chem. Glasses* **1992**, *33*, 149.
[39] I. Ardelean, E. Burzo, D. Mitulescu, S. Simion, *J. Non-Cryst. Solids* **1992**, *146*, 256.
[40] B. Sreedhar, P. Indira, A. K. Bhatnagar, *Ind. J. Pure Appl. Phys.* **1995**, *33*, 353.
[41] E. Culea, A. Pop, I. Cosma, *J. Magn. Magn. Mater.* **1996**, *157/158*, 163.
[42] T. Ristoiu, E. Culea, I. Bratu, *Mater. Lett.* **1999**, *41*, 135.
[43] H. J. A. Kooppmans, M. M. A. Perik, B. Nieuwenhuijse, P. J.Gellings, *Phys. Status Solidi B* **1983**, *120*, 745.
[44] I. V. Chepeleva, V. N. Lazukin, *Dokl. Akad. Nauk. SSSR* **1976**, *226*, 311.
[45] D. L. Griscom, *J. Non-Cryst. Solids* **1980**, *40*, 211.
[46] C. M. Brodbeck, L. E. Iton, *J. Chem. Phys.* **1985**, *83*, 4285.
[47] C. Brecher, L. A. Riseberg, *Phys. Rev. B* **1980**, *21*, 2607.
[48] E. Beuchler, J. Turkevich, *J. Phys. Chem.* **1972**, *76*, 2325.
[49] J. Reuben, *J. Chem. Phys.* **1971**, *75*, 3164.
[50] J. H. Freed, *J. Chem. Phys.* **1978**, *68*, 4034.

  0947-6539/02/0822-5130 $ 20.00+.50/0

[51] D. H. Powell, O. M. Ni Dhubhghaill, D. Pubanz, L. Helm, Y. S. Lebedev, W. Schlaepfer, A. E. Merbach, *J. Am. Chem. Soc.* **1996**, *118*, 9333.
[52] J. Kärger, H. Pfeifer, E. Riedel, H. Winkler, *J. Colloid Interface Sci.* **1973**, *44*, 187.
[53] A. C. McLaughlin, J. S. Leigh, Jr. *J. Magn. Reson.* **1973**, *9*, 296.
[54] J. S. Leigh, Jr., *J. Magn. Reson.* **1971**, *4*, 308.
[55] C. F. Hazlewood, D. C. Chang, B. L. Nichols, D. E. Woessner, *Biophys. J.* **1974**, *14*, 583.
[56] I. Solomon, *Phys. Rev.* **1955**, *99*, 559.
[57] N. Bloembergen, L. O. Morgan, *J. Chem. Phys.* **1961**, *34*, 842.
[58] D. H. Powell, A. E. Merbach, G. González, E. Brücher, K. Micskei, M. F. Ottaviani, K. Köhler, A. Von Zelewsky, O. Y. Grinberg, Y. S. Lebedev, *Helv. Chim. Acta* **1993**, *76*, 2129.
[59] A. D. McLachlan, *Proc. R. Soc. London Ser. A* **1964**, *280*, 271.
[60] F. J. Berry, M. Carbucicchio, A. Chiari, C. Johnson, E. A. Moore, M. Mortimer, F. F. F. Vetel, *J. Mater. Chem.* **2000**, *10*, 2131.
[61] R. B. Clarkson, A. I. Smirnov, T. I. Smirnova, R. L. Belford in *The Chemistry of Contrast Agents in Medical Magnetic Resonance Imaging* (Eds.: A. E. Merbach, É. Tóth), Wiley, Chichester, **2001**, Chapter 9, pp. 383–415.
[62] É. Tóth, L. Helm, A. E. Merbach in *The Chemistry of Contrast Agents in Medical Magnetic Resonance Imaging* (Eds.: A. E. Merbach, É. Tóth), Wiley, Chichester, **2001**, Chapter 2, pp. 45–119.
[63] W. D. Basler, *Ber. Bunsenges. Phys. Chem.* **1978**, *82*, 1051.
[64] H. G. Jiang, M. Rühle, E. J. Lavernia, *J. Mater. Res.* **1999**, *14*, 549.

Received: March 4, 2002 [F3924]

  0947-6539/02/0822-5131 $ 20.00+.50/0